Geochemistry Geophysics Geosystems G3
AN ELECTRONIC JOURNAL OF THE EARTH SCIENCES
Published by AGU and the Geochemical Society

Article
Volume 3, Number 1
XX Month 2002
10.1029/2001GC000222
ISSN: 1525-2027

Timescales for the evolution of seismic anisotropy in mantle flow

Édouard Kaminski and Neil M. Ribe

Laboratoire de Dynamique des Systèmes Géologiques, IPG Paris, 4 Place Jussieu, 75252 Paris cédex 05, France (kaminski@ipgp.jussieu.fr; ribe@ipgp.jussieu.fr)

[1] We study systematically the relationship between olivine lattice preferred orientation and the mantle flow field that produces it, using the plastic flow/recrystallization model of *Kaminski and Ribe* [2001]. In this model, a polycrystal responds to an imposed deformation rate tensor by simultaneous intracrystalline slip and dynamic recrystallization, by nucleation and grain boundary migration. Numerical solutions for the mean orientation of the *a* axes of an initially isotropic aggregate deformed uniformly with a characteristic strain rate $\dot{\epsilon}$ show that the lattice preferred orientation evolves in three stages: (1) for small times $t \leq 0.2\dot{\epsilon}^{-1}$, recrystallization is not yet active and the average *a* axis follows the long axis of the finite strain ellipsoid; (2) for intermediate times $0.2\dot{\epsilon}^{-1} \leq t \leq 1.0\dot{\epsilon}^{-1}$, the fabric is controlled by grain boundary migration and the average *a* axis rotates toward the orientation corresponding to the maximum resolved shear stress on the softest slip system; (3) for $1.0\dot{\epsilon}^{-1} \leq t \leq 3.0\dot{\epsilon}^{-1}$, the fabric is controlled by plastic deformation and average *a* axis rotates toward the orientation of the long axis of the finite strain ellipsoid corresponding to an infinite deformation (the "infinite strain axis".) In more realistic nonuniform flows, lattice preferred orientation evolution depends on a dimensionless "grain orientation lag" parameter $\Pi(\mathbf{x})$, defined locally as the ratio of the intrinsic lattice preferred orientation adjustment timescale to the timescale for changes of the infinite strain axis along path lines in the flow. Explicit numerical calculation of the lattice preferred orientation evolution in simple fluid dynamical models for ridges and for plume-ridge interaction shows that the average *a* axis aligns with the flow direction only in those parts of the flow field where $\Pi \ll 1$. Calculation of Π provides a simple way to evaluate the likely distribution of lattice preferred orientation in a candidate flow field at low numerical cost.

Components: XXX words, 9 figures.

Received 29 August 2001; **Revised** 18 January 2002; **Accepted** 4 April 2002; **Published** XX Month 2002.

Kaminski, É., and N. L. M. Ribe, Timescales for the evolution of seismic anisotropy in mantle flow, *Geochem. Geophys. Geosyst.*, *3*(1), 10.1029/2001GC000222, 2002.

1. Introduction

[2] Since the early observations of *Hess* [1964], it has been well established that much of the upper mantle (above 400 km) is seismically anisotropic [e.g., *Montagner*, 1994]. This anisotropy is usually attributed to the lattice preferred orientation (LPO) of anisotropic olivine crystals [*Nicolas and Christensen*, 1987; *Montagner*, 1998]. The fact that lattice preferred orientation is in turn produced by flow has led seismologists routinely to interpret the direction of anisotropy as an indicator of the flow

direction in the mantle [e.g., *Russo and Sylver*, 1994]. However, the conditions under which this assumption is valid remain to be established [*Savage*, 1999]. To this end, we propose here a new quantitative description of the relationship between seismic anisotropy and mantle flow, with emphasis on the characteristic timescales involved.

[3] When a crystal is subject to an externally imposed deformation, it responds primarily by intracrystalline slip on given active slip systems [e.g., *Poirier*, 1985]. In a polycrystal, intracrystalline slip is a function of the orientation of the grains relative to the externally imposed stress and depends on the compatibility of deformation between neighboring grains [*Etchecopar*, 1977]. The rotation of the crystallographic axes induced by intracrystalline slip is therefore a function of crystal orientation, which leads to a lattice preferred orientation in the aggregate. Modeling of plastic deformation in olivine polycrystals has provided important insight into the link between seismic anisotropy and mantle flow [*Wenk et al.*, 1991; *Ribe and Yu*, 1991; *Chastel et al.*, 1993; *Tommasi et al.*, 2000]. Although these models differ in their treatment of such matters as stress and/or strain compatibility, they all predict that the lattice preferred orientation of an initially isotropic aggregate deformed uniformly follows the finite strain ellipsoid (FSE), with the fast axis of olivine aligned with the longest axis of the finite strain ellipsoid [*Wenk et al.*, 1991; *Ribe*, 1992]. These predictions agree well with experimental observations at small strain in both simple shear [*Zhang and Karato*, 1995] and uniaxial compression [*Nicolas et al.*, 1973].

[4] However, the experiments of *Zhang and Karato* [1995] show that at large strain, the mean *a* axis orientation no longer follows the finite strain ellipsoid but rotates more rapidly toward the shear direction. This evolution is accompanied by intensive dynamic recrystallization, by subgrain rotation (SGR) and grain boundary migration (GBM) [*Zhang et al.*, 2000]. The experiments of *Nicolas et al.* [1973] similarly indicate that the evolution of the lattice preferred orientation at large strains is controlled by dynamic recrystallization. Because finite strains are large in the convecting mantle [*McKenzie*, 1979], dynamic recrystallization is likely to control the lattice preferred orientation there. A model for dynamic recrystallization of olivine is thus required for interpreting observations of anisotropy in terms of mantle flow.

[5] Two models are now available for the evolution of olivine lattice preferred orientation by simultaneous plastic flow and recrystallization: the viscoplastic model of *Wenk and Tomé* [1999], and the kinematic-hybrid model of *Kaminski and Ribe* [2001]. In the latter model, which we shall use in this study, the shear rates on the active slip systems of all grains in an aggregate are calculated by minimizing the difference between the imposed external deformation rate tensor and the deformation rate tensors within the grains themselves. Plastic flow in turn increases the dislocation density within each grain at a rate proportional to the resolved shear stresses on the various slip systems (Schmidt factors). Grains oriented favorably relative to the imposed stress field (“soft” grains) will thus achieve higher dislocation densities than unfavorably oriented (“hard”) ones [*Karato and Lee*, 1999]. Grains with a large density of dislocations tend to polygonize, forming strain-free nuclei by subgrain rotation and thereby lowering their bulk strain energy [*Poirier*, 1985]. Grains with low strain energy then invade grains with higher energy by grain boundary migration [*Karato*, 1987].

[6] In *Kaminski and Ribe* [2001], subgrain rotation and grain boundary migration are quantified by two dimensionless parameters: the nucleation rate λ^* of strain-free subgrains and the grain-boundary mobility M^*, the values of which can be obtained by comparison with experiments. Many simple shear experiments are now available to constrain the values of the parameters of dynamic recrystallization [*Zhang et al.*, 2000; *Bystricky et al.*, 2000]. They indicate that $\lambda^* = 5$ and that M^* lie between 50 and 200 as a function of temperature [*Kaminski and Ribe*, 2001]. Comparison with the experiment in uniaxial compression of *Nicolas et al.* [1973] yields to $\lambda^* = 5$ and $M^* = 50$ [*Kaminski and Ribe*, 2001]. These latter values are thus in agreement with the two sets of experiments (Figure 1) and will be used as reference values in the following. For this set of parameters, soft grains have a large probability of

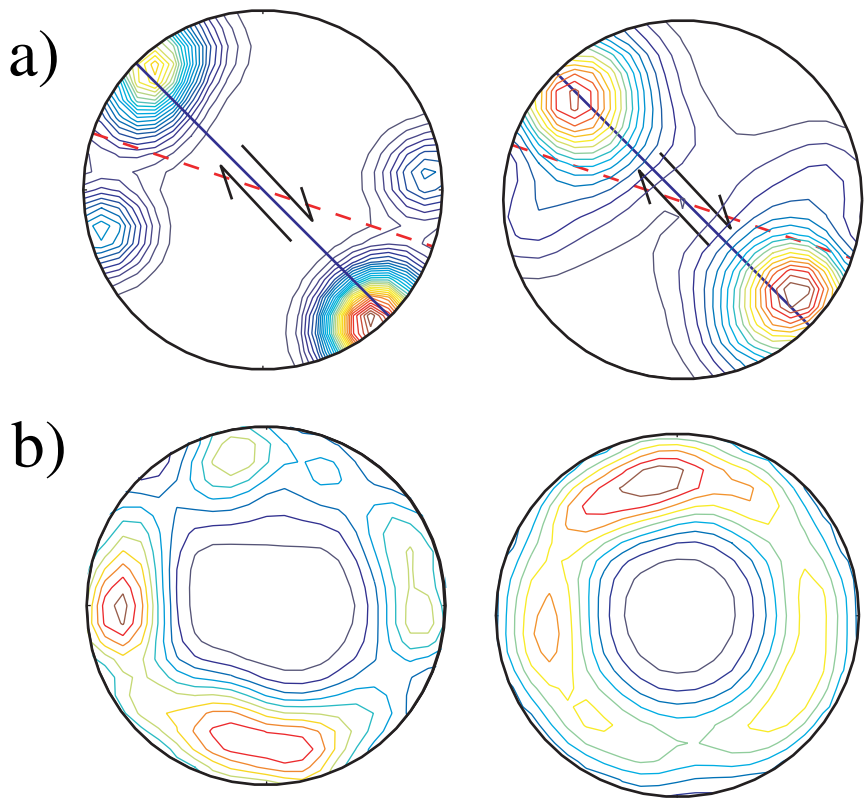

Figure 1. Pole figures (Lambert equal-area projection, contours at 0.1 times a random distribution) of the *a* crystallographic axes of olivine, in the reference frame defined by the principal axes of the strain rate tensor. The left diagram corresponds to laboratory experiments and the right diagram gives the model prediction for the same deformation and for $\lambda^* = 5$ and $M^* = 50$. (a) Simple shear experiments [*Zhang and Karato*, 1995], 150% finite strain. The solid line represents the shear plane and the dashed line the foliation. (b) Uniaxial compression [*Nicolas et al.*, 1973], 58% shortening. The shortening direction is at the center of the diagrams [from *Kaminski and Ribe*, 2001].

nucleation and thus on average a low strain energy. They are thus favored by grain boundary migration and dominate the lattice preferred orientation.

[7] In this article, we first present the predictions of the model for simple uniform deformations, for which analytical results can be used to interpret physically the lattice preferred orientation evolution. We will then consider more complex "mantle-flow-like" deformations to derive geophysically relevant conclusions.

2. LPO Development for Uniform Deformations

[8] In *Kaminski and Ribe* [2001], the plastic deformation experienced by the crystals in an aggregate depends only on the deformation imposed externally by the large-scale flow field. This deformation is described by a velocity gradient tensor

$$L_{ij} = \frac{\partial v_i}{\partial x_j} = E_{ij} - \varepsilon_{ijk}\Omega_k, \tag{1}$$

where v_i is the Eulerian velocity vector, x_j is the vector of Eulerian coordinates, E_{ij} is the strain rate tensor, $2\Omega_k$ is the vorticity vector, and ε_{ijk} is the alternating tensor. For a given material aggregate embedded in an arbitrary flow field, L_{ij} will be a function of time in general. Dynamic recrystallization depends on the density of dislocations in the aggregate, which in the model of *Kaminski and Ribe* [2001] depends only on the orientation of the grains relative to E_{ij}. As a consequence, the lattice preferred orientation due to both plastic deformation and dynamic recrystallization depends only on

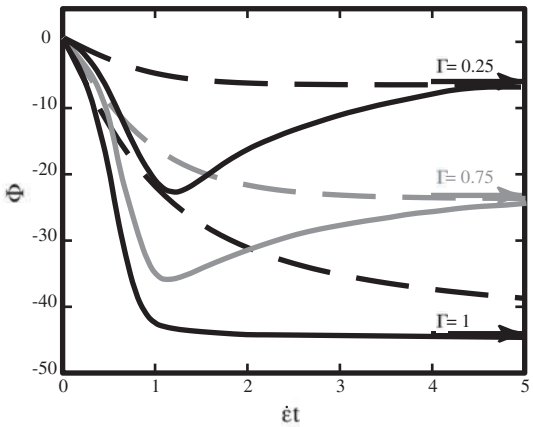

Figure 2. Evolution of the mean orientation Φ of olivine *a* axes relative to the extension direction (in the reference frame defined by the eigen vectors of the strain rate tensor) in an initially isotropic aggregate as a function of strain $\dot{\epsilon}t$ for three different uniform planar deformations (Γ = 0.25, 0.75, and 1.) The solid curves show the orientation of the *a* axes and the dashed curves show the orientation of the long axis of the finite strain ellipsoid. The average *a* axis tends toward the infinite strain axis orientation (arrows) in three distinct stages (see text.)

the initial lattice preferred orientation of the aggregate and on the deformation history $L_{ij}(t)$. The evolution is particularly simple if the initial lattice preferred orientation is isotropic and the deformation is uniform (i.e., L_{ij} is constant).

2.1. Plane Strain Deformations

[9] Consider first the case of uniform incompressible plane strain deformation, for which the the only nonzero rates of strain are $E_{11} = -E_{22} = \dot{\epsilon}$. There may also be a rotational component of magnitude $|\Omega|$ about the x_3 axis, defining a dimensionless "vorticity number" $\Gamma = \Omega/\dot{\epsilon}$. Pure shear corresponds to $\Gamma = 0$ and simple shear to $\Gamma = \pm 1$.

[10] The model of *Kaminski and Ribe* [2001] reproduces the observation of *Zhang and Karato* [1995] that the lattice preferred orientation of an olivine aggregate deformed in simple shear initially follows the finite strain ellipsoid and then rotates more rapidly toward the shear plane. We now use the same model to study the evolution of the lattice preferred orientation for an arbitrary vorticity number. Figure 2 shows the evolution of the lattice preferred orientation predicted by the model of *Kaminski and Ribe* [2001] with $\lambda^* = 5$ and $M^* = 50$ for three different vorticity numbers (Γ = 0.25, 0.75, 1.0), together with the orientation ψ_{FSE} of the long axis of the finite strain ellipsoid [*McKenzie*, 1979, equation (28)],

$$\psi_{FSE} = \frac{1}{2}\tan^{-1}\left[\frac{\Gamma \tanh\left(\sqrt{1-\Gamma^2}\dot{\epsilon}t\right)}{\sqrt{1-\Gamma^2}}\right]. \qquad (2)$$

[11] The lattice preferred orientation evolves in three distinct stages. (1) At an early transient stage ($\dot{\epsilon}t \leq 0.2$) the lattice preferred orientation follows the finite strain ellipsoid as predicted by purely intracrystalline deformation, indicating that plastic deformation is dominant. (2) Later ($1.2 \geq \dot{\epsilon}t \geq 0.2$), the lattice preferred orientation evolves faster than the finite strain ellipsoid, which reflects the influence of dynamic recrystallization. *Kaminski and Ribe* [2001] and *Wenk and Tomé* [1999] have shown that grain boundary migration combined with subgrain rotation induces the growth of the grains in the "softest" orientation, for which the resolved shear stress applied on the softest slip system is maximal. The resolved shear stress on a slip plane in a crystal is proportional to the scalar $I \equiv l_i n_j E_{ij}$ where n_j and l_i are the unit vectors normal to the plane and in the slip direction, respectively [*Ribe and Yu*, 1991]. I depends only on the orientation of the grain relative to the principal axes of the strain rate tensor and hence does not depend on the vorticity. In Figure 2, the softest orientation (largest I) is $-45°$, which coincides with the direction of shearing for simple shear. The second phase of the lattice preferred orientation evolution reflects the increasing volume fraction of the grains in the softest orientation. If only grain boundary migration were active, the lattice preferred orientation would eventually become concentrated at this orientation. However, because plastic deformation continues to be active, the actual evolution exhibits an additional stage. (3) In the third stage ($\dot{\epsilon}t \geq 1.2$) the grains rotate away from the softest orientation and reach a steady-state orientation as the rotation becomes slower and slower at large strain. Because the

rotation rate of a crystal in the softest orientation is $(1 - |\Gamma|)\dot{\epsilon}$ [from *Kaminski and Ribe*, 2001, equation (8)], the grains in the softest orientation will always rotate away from it except in the special case of simple shear. The volume fraction of grains in the softest orientation increases by grain boundary migration but decreases by plastic rotation. The global rotation of the lattice preferred orientation reflects the growing dominance of plastic deformation over grain boundary migration as the lattice preferred orientation sharpens and the differences of strain energy (and hence the rate of grain boundary migration) decrease in the aggregate. Once plastic deformation has become dominant it determines the rotation of the lattice preferred orientation toward an apparent steady state. Figure 2 suggests that the final steady-state *a* axis orientation coincides with the asymptotic orientation of the long axis of the finite strain ellipsoid in the limit of infinite strain ($t \rightarrow \infty$), which we shall call the "infinite strain axis" (ISA). For plane strain deformations, the orientation ψ_{ISA} of the infinite strain axis relative to the axis of maximum instantaneous extension is found from equation (2) as

$$\psi_{ISA} = \lim_{\epsilon \to \infty} \psi_{FSE} = \frac{1}{2}\sin^{-1}\Gamma. \tag{3}$$

[12] Note from equation (3) that the infinite strain axis is not defined for $|\Gamma| > 1$. In that case, neither the finite strain ellipsoid nor the lattice preferred orientation reaches a steady state: both continue to spin around even at infinite strain.

[13] Plastic deformation introduces only one timescale, $1/\dot{\epsilon}$ [*Ribe*, 1992], whereas three timescales can be defined here for the evolution of the average *a* axes orientation Φ. (1) The smallest timescale, τ_{FSE}, corresponds to the first stage in which Φ follows the long axis of the finite strain ellipsoid. The τ_{FSE} is the time necessary for plastic deformation to build up heterogeneities of strain energy in the aggregate large enough to drive grain boundary migration. We define τ_{FSE} as the time at which the difference between Φ and ψ_{FSE} reaches 1° degree. Numerical calculations show that τ_{FSE} mainly depends on Γ whereas its dependence on λ^* and M^* is negligible. For $\lambda^* = 5$ and M^* between 50 and 200, its total range of variation for arbitrary Γ is

$$\tau_{FSE} = \frac{0.2 \pm 0.1}{\dot{\epsilon}}. \tag{4}$$

(2) The intermediate timescale, τ_{GBM}, corresponds to the second stage in which Φ rotates toward the softest orientation. The τ_{GBM} is the time necessary for grain boundary migration to level down strain heterogeneities enough for grain boundary migration to be less efficient than plastic deformation. We define τ_{GBM} as the time at which Φ is minimum (see Figure 2). At this point, the effects of grain boundary migration and of plastic deformation just balance each other. The τ_{GBM} is a complex function of both λ^*, M^*, and Γ. For $\lambda^* = 5$ and M^* between 50 and 200, its total range of variation for arbitrary Γ is

$$\tau_{GBM} = \frac{1.0 \pm 0.5}{\dot{\epsilon}}. \tag{5}$$

(3) The largest timescale, τ_{ISA}, corresponds to the third stage, in which Φ approaches the infinite strain axis. The τ_{ISA} is the time necessary for the grains to rotate plastically from the softest orientations (previously nourished by grain boundary migration) toward the infinite strain axis. We define τ_{ISA} as the time at which the difference between the infinite strain axis orientation and Φ is less than 2°. Figure 3 gives the variation of τ_{ISA} as a function of the vorticity number for $4 \leq \lambda^* \leq 8$ and for $50 \leq M^* \leq 200$. Numerical solutions show that τ_{ISA} is largely independent of λ^* and M^*. The total range of variations of τ_{ISA} is

$$\tau_{ISA} = \frac{3.0 \pm 2.5}{\dot{\epsilon}}. \tag{6}$$

[14] The fastest evolution ($\tau_{ISA} = 0.5$) is obtained for $\Gamma = \pm 1$ and $M^* = 200$ and the slowest evolution ($\tau_{ISA} = 5.5$) for $\Gamma = \pm 0.5$ and $M^* = 50$.

[15] As the strains are large in the convective mantle, the first stage ($t \leq \tau_{FSE}$) is of limited importance. In the second stage ($t \leq \tau_{GBM}$) the lattice preferred orientation is influenced by both grain boundary migration and plastic deformation and can thus vary greatly as a function of strain. In

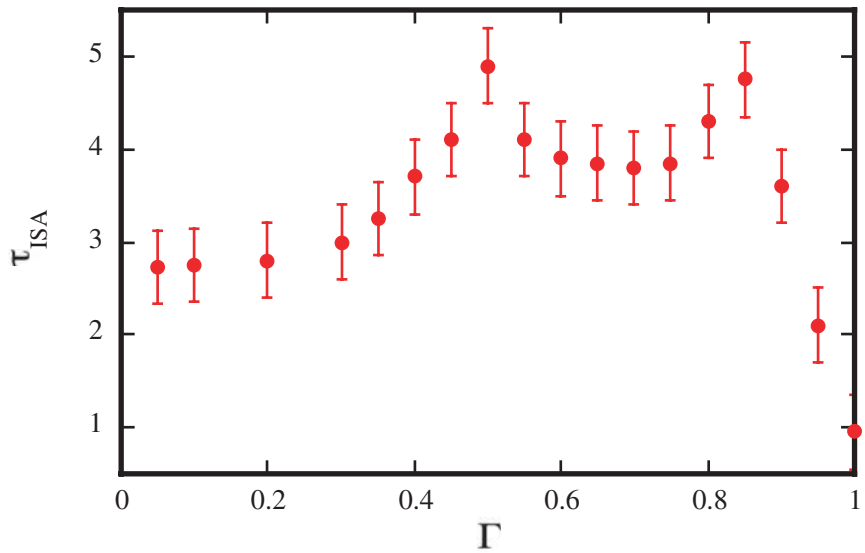

Figure 3. Average value of τ_{ISA}, the time required for the *a* axes to reach the infinite strain axis, as a function of Γ. The error bars give the range of values for τ_{ISA} at a given vorticity number for λ* between 4 and 8 and *M** between 50 and 200.

this stage, the average *a* axis of an aggregate will only coincidentally align with the flow direction. Only in the third stage, when the mean *a* axes orientation reaches a steady state defined by the infinite strain axis, may the crystals be aligned with the flow direction, and then only if the infinite strain axis is itself aligned with the flow direction. The relevant timescale for the interpretation of seismic anisotropy is thus τ_{ISA}. We now characterize τ_{ISA} for arbitrary deformation.

2.2. Three-Dimensional Deformations

[16] The three-stage evolution of lattice preferred orientation documented above for uniform plane strain deformations occurs also for uniform three-dimensional (3-D) deformations. In particular, numerical solutions for various choices of L_{ij} confirm our hypothesis that the mean *a* axis orientation approaches the infinite strain axis (when it exists) in the limit of infinite strain. In a 3-D flow, the infinite strain axis at a given point is just the orientation of the long axis of the finite strain ellipsoid produced by deforming a material sphere at the rate L_{ij} for an infinite time. Unfortunately, no analytical representation of the dependence of the infinite strain axis on the components of L_{ij} is available for a general uniform 3-D flow. We therefore have devised a simple numerical procedure to test for the existence of the infinite strain axis and to calculate it when it exists (appendix A.)

[17] As for the case of plane strain, the time required for the mean *a* axis orientation to reach the infinite strain axis is $\tau_{ISA} \sim \dot{\epsilon}^{-1}$, where $\dot{\epsilon}$ is the absolute value of the largest eigenvalue of the strain rate tensor. However, τ_{ISA} also depends on several other parameters, including the vorticity number and the orientation of the vorticity vector relative to the principal strain rate axes. Rather than attempt to determine the complete dependence of τ_{ISA} on these parameters, we simply determined numerically the range of its variation for a variety of uniform 3-D flows and for $50 \leq M^* \leq 250$. We find that τ_{ISA} is mainly a function of the magnitude of the vorticity vector. As a consequence, it always falls in the range given by (equation (6)).

[18] The infinite strain axis is controlled by the velocity gradient tensor and therefore need not be directly related to the velocity vector itself. To see this, consider planar flows with Γ = 1.0 (simple shear), 0 (pure shear), and 0.5 (intermediate.) Figure 4 shows the streamlines for these flows, together with the orientations of the softest grains and the infinite strain axis. The softest grain orientation is the same for all three flows because it

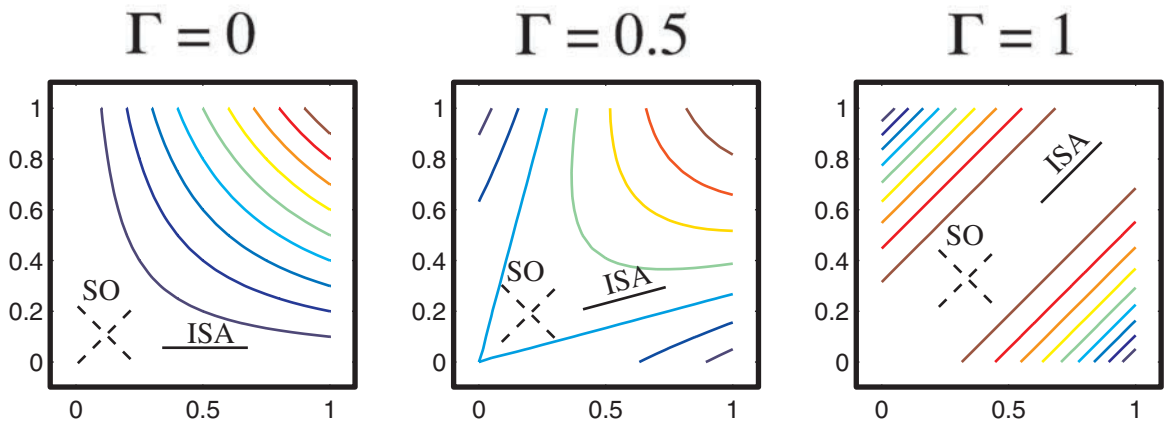

Figure 4. Contours of the stream function (equivalent to streamlines, arbitrary units) for three plane strain flows with uniform velocity gradient tensor L_{ij} and three values of the vorticity number Γ. The horizontal and vertical axes are the directions of maximum extension and shortening rates, respectively. The orientations of the infinite strain axis (ISA) and the softest grain orientation (SO) are shown. For a given finite strain, the mean *a* axis orientation will lie between the softest grain orientation and the infinite strain axis. Only for Γ = 1.0 (simple shear) are the infinite strain axis and the softest grain orientation, and thus the *a* axes, aligned everywhere with the local flow direction.

depends only on the strain rate tensor and not on the vorticity. In general, there is no simple relationship between either the softest grain orientation or the infinite strain axis and the flow direction. Only in the case of simple shear (Γ = 1) do all three orientations coincide everywhere in the flow field. For other values of Γ, the mean *a* axis of an aggregate following a streamline will rotate from the softest grain orientation toward the infinite strain axis orientation, which itself is only aligned with the flow direction at isolated points. Consequently, the lattice preferred orientation will not in general be aligned with the flow direction even for uniform deformations, except for the special case of simple shear.

3. LPO Adjustment Along Path Lines

[19] So far we have considered only uniform deformations whose sole intrinsic timescale is a typical inverse strain rate $\dot{\epsilon}^{-1}$. Most realistic flows, however, are both spatially nonuniform and time-dependent. In such flows, an aggregate traveling along a pathline (= streamline if the flow is steady) will "feel" a velocity gradient tensor $L_{ij}(t)$ that changes with time. The rate of this change introduces a new timescale which plays an important role in controlling lattice preferred orientation evolution.

[20] In a nonuniform flow, the lattice preferred orientation can be aligned with the flow direction only if two conditions are fulfilled: (1) the infinite strain axis itself is aligned with the flow direction and (2) the rate of change of the infinite strain axis orientation along the path line is slow enough for the lattice preferred orientation to "adjust" to it. We first focus on the second condition, which in some cases is both necessary and sufficient (appendix B.) To quantify this condition, we introduce a dimensionless "grain orientation lag" (GOL) parameter

$$\Pi \equiv \frac{\tau_{\mathrm{ISA}}}{\tau_{\mathrm{flow}}}, \tag{7}$$

where τ_{ISA} and τ_{flow} are the timescales for crystal rotation toward the infinite strain axis and for changes of the infinite strain axis orientation itself along path lines, respectively. If $\Pi \ll 1$, the along path line variation of the infinite strain axis orientation is much slower than crystal rotation, and the lattice preferred orientation will quickly become aligned with the local infinite strain axis. The opposite situation obtains if $\Pi \gg 1$: crystal rotation is then unable to keep up with the rapid changes of the infinite strain axis, leading to an lattice preferred orientation that depends in a complex way on the deformation history.

[21] We know already that $\tau_{\mathrm{ISA}} \sim \dot{\epsilon}^{-1}$. A suitable measure of τ_{flow} is the inverse rate of change of the

angle $\Theta \equiv \cos^{-1}(\hat{u} \cdot \hat{e})$ between the local flow direction $\hat{u} = \vec{u}/|u|$ and the local ISA $\hat{e}$:

$$\tau_{\text{flow}} = \left|\frac{\mathrm{D}\Theta}{\mathrm{D}t}\right|^{-1}, \tag{8}$$

where $\mathrm{D}/\mathrm{D}t \equiv \partial/\partial t + \vec{u} \cdot \nabla$ is the material derivative. Equation (7) now becomes

$$\Pi = \frac{1}{\dot{\epsilon}}\left|\frac{\mathrm{D}\Theta}{\mathrm{D}t}\right|. \tag{9}$$

[22] The grain orientation lag $\Pi = \Pi(\vec{x}, t)$ is a purely local parameter whose value will in general depend on position (and on time if the flow is unsteady). If $\Pi = 0$, the angle between the flow direction and infinite strain axis is constant along a path line in the neighborhood of the point in question. If this angle is furthermore equal to zero, then the infinite strain axis will coincide with the local flow direction. The condition $\Pi = 0$ is thus a necessary condition for the *a* axis of olivine to be aligned with the flow direction. To verify that this condition is also sufficient requires a complete calculation of the lattice preferred orientation evolution along path lines, which we now carry out for two model geophysical flows.

4. Geophysical Examples

4.1. Corner Flow

[23] We illustrate the variability of Π for a corner flow, which is a simple model for the mantle flow under a ridge axis. Let U be the half spreading rate, and let (r, θ) be polar coordinates with origin at the ridge axis such that $\theta = 0$ is vertical. The equations of slow viscous flow admit a similarity solution in which the velocity $\vec{u}$ is a function of θ only [*Batchelor*, 1967, p. 224]:

$$\vec{u} \cdot \hat{r} = \frac{2U}{\pi}(\theta \sin\theta - \cos\theta), \qquad \vec{u} \cdot \hat{\theta} = \frac{2U}{\pi}\theta\cos\theta. \tag{10}$$

[24] To apply this model to the Earth, we suppose that $\theta = \pi/2$ corresponds to the Earth's surface while $z = r\cos\theta = 1$ is the depth of the phase change α olivine to β spinel. We suppose that the aggregates are isotropic at that depth and follow the evolution of the lattice preferred orientation along four path lines. The lattice preferred orientation evolves by plastic deformation and dynamic recrystallization with $\tilde{M} = 50$ and $\lambda^* = 5$.

[25] Figure 5 shows schematically the mean orientation of the fast ([100]) axis of olivine, together with contours of Π, which for the corner flow is

$$\Pi = \frac{\theta(\theta^2 + \cos^2\theta)}{\tan\theta(\theta^2 + \cos^2\theta - \theta\sin 2\theta)}. \tag{11}$$

When $\Pi > 0.5$, the lattice preferred orientation is a function of the deformation history, displays secondary peaks, and shows large variations both along and between streamlines. When $\Pi < 0.5$, secondary peaks vanish and the lattice preferred orientation rotates towards the flow direction. Finally, when $\Pi < 0.1$, the mean *a* axis orientation is essentially aligned with the flow direction. The parameter Π thus gives a good preliminary picture of the likely anisotropic structure of the flow and identifies those regions where a complete calculation of the lattice preferred orientation is necessary.

4.2. Plume/Ridge Interaction

[26] We now turn to an example of a fully 3-D flow: the interaction between a plume and a spreading ridge. The flow due to the ridge is the corner flow considered in the previous subsection. The plume is represented by a buoyant cylinder of radius R, length L, and density deficit $\Delta\rho$, which drives flow in a half-space of fluid with viscosity μ beneath a no-slip surface $z = 0$. The total velocity is just the sum of the ridge and plume components and has the form

$$\vec{u}(x, y, z) = U\vec{f}_r(\theta) + \frac{g\Delta\rho R^2}{\mu}\vec{f}_p\left(\frac{r_1}{R}, \frac{z}{R}, \frac{L}{R}\right), \tag{12}$$

where g is the acceleration of gravity at the surface, $r_1 = \sqrt{(x - x_o)^2 + y^2}$ is the lateral distance from the plume axis, x_o is the distance from the plume axis to the ridge, and $\vec{f}_r$ and $\vec{f}_p$ are the dimensionless velocity fields associated with the ridge and the plume, respectively. The plume flow $\vec{f}_p$ is calculated as by *Ribe and Christensen* [1999] by representing the buoyant cylinder as a distribution of Stokeslets with additional singular solutions added to satisfy the no-slip boundary condition

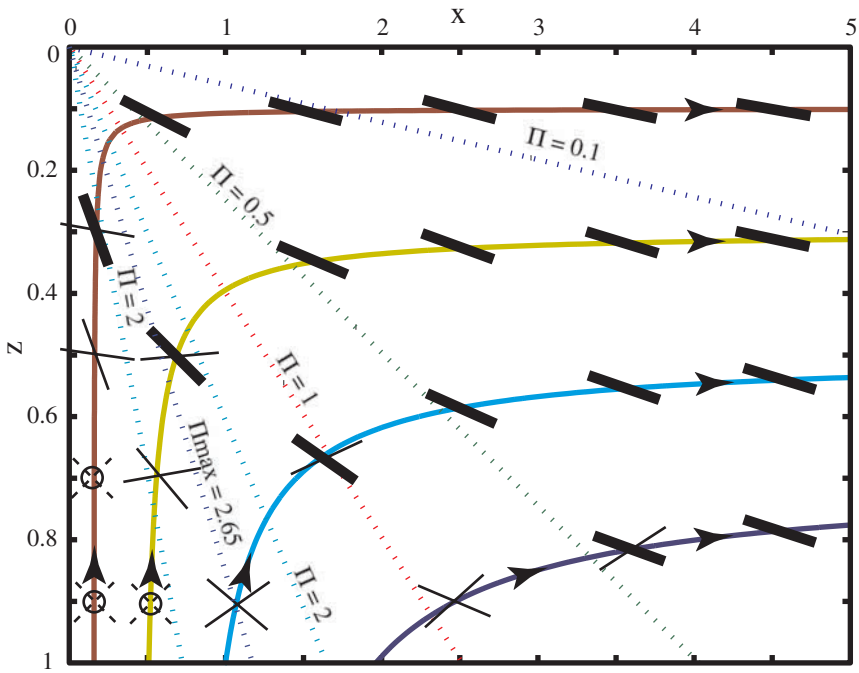

Figure 5. Evolution of lattice preferred orientation along four path lines in a corner flow, starting from an isotropic lattice preferred orientation at $z = 1$. Dotted lines are contours of the grain orientation lag parameter Π defined by (equation (9)). The small heavy bars give the peak orientation of the *a* axis, while the light bars give the orientation of the weak secondary peak when present. Dashed bars with circle indicate no preferred orientation. The lattice preferred orientation is aligned with the flow direction when $\Pi \ll 1$, but there is no relationship between the two when $\Pi > 0.5$.

[*Podzrikidis*, 1997, p. 255]. The total (ridge plus plume) velocity thus satisfies the spreading ridge boundary condition $\vec{u}(x, y, 0) = 2U[H(x) - 1/2]\hat{x}$, where $H(x)$ is the Heaviside step function.

[27] Figure 6 shows the streamlines of the flow in the vertical plane of symmetry $y = 0$ (normal to ridge and containing the plume axis), for $x_o = 7.5R$ and $L = 6R$. Interaction of the ridge and plume flows produces the region of counterflow at the top between the ridge and the buoyant cylinder. Although the density anomalies are not advected by the flow in this simple model, it is still useful to characterize the plume's strength in terms of a nominal "buoyancy flux" B through the lower surface of the cylinder:

$$B = -2\pi \frac{g\Delta\rho^2 R^2}{\mu} \int_0^R r_1 \vec{f}_p\left(\frac{r_1}{R}, \frac{L}{R}, 6\right) \cdot \hat{z} \mathrm{d}r_1 = 1.22 \frac{g\Delta\rho^2 R^4}{\mu}. \quad (13)$$

For example, using $\mu = 10^{20}$ Pa s, $R = 70$ km, and $\Delta\rho = 40$ kg m^{-3} gives $B = 3100$ kg s^{-1}, a value similar to that inferred for Hawaii [*Ribe and Christensen*, 1999].

[28] Figure 7 shows the horizontal structure of the plume-ridge flow at a "mid-asthenospheric" depth $z = 0.5R$. Blue arrows indicate the horizontal velocity, and the red bars show the horizontal projection of the mean *a* axes orientation in the aggregate. The lattice preferred orientation was calculated numerically with $\lambda^* = 5$ and $M^* = 50$, assuming initial isotropy at $z = 6R$ for all streamlines. The roughly parabolic pattern of the velocity vectors around the plume is due to the deflection of the axisymmetric plume flow by the rightward plate-driven flow. The lattice preferred orientation is nearly aligned with the flow direction far from the ridge and the plume but is not so aligned closer to them. This result can be interpreted with the aid of Figure 8, which shows the orientation lag parameter $\Pi(x, y)$ at the same depth ($z = 0.5R$), calculated using the procedure described in appendix A. Three zones appear clearly in Figures 7 and 8: (1) Near the ridge axis, Π is large because the flow changes abruptly from mainly

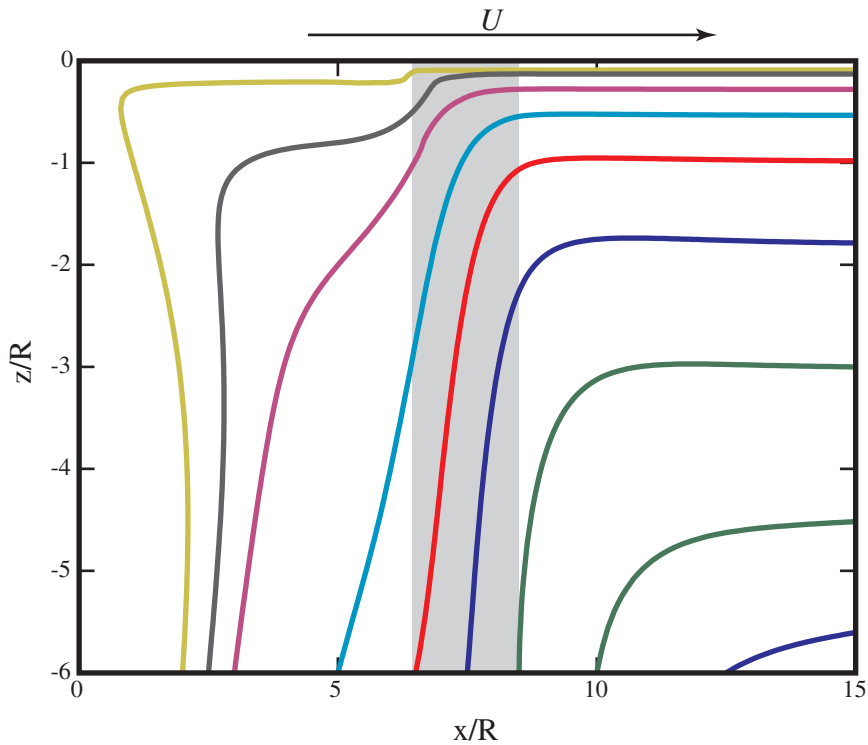

Figure 6. Streamlines (arbitrary contour intervals) in the vertical symmetry plane $y = 0$ for the flow produced by a buoyant cylinder of radius R (grey) near a spreading ridge with half spreading rate U ($x = 0$), determined as described in the text.

vertical to mainly horizontal. The lattice preferred orientation cannot follow this rapid change and is normal to the flow direction. (2) Far from the plume and the ridge, the flow direction changes smoothly, Π is small, and the lattice preferred orientation is aligned with the flow direction. (3) Closer to the plume, the flow is disrupted, leading to large values of Π and lattice preferred orientation poorly aligned with the flow direction. Π is large in the region of counterflow in front of the plume and in most of the parabolic region defined by the velocity vectors (Figure 7) The large variations of Π around the plume indicate a deformation state close to uniaxial compression ($E_{11} \approx E_{22}$), for which numerical calculation of the infinite strain axis is not stable. In the core of the plume (black), Π is not defined because the vorticity is large. As for the simpler corner-flow example, we conclude that $\Pi < 0.5$ is a necessary condition for the lattice preferred orientation to be aligned with the flow direction. A complete calculation is required to determine the lattice preferred orientation in regions where Π is larger.

[29] We close this section with a simple direct calculation of the radial seismic anisotropy implied by our plume-ridge model. Radial anisotropy is of particular interest because it is independent of azimuth and can be retrieved with good resolution from Rayleigh and Love wave data if the anisotropy is small [*Montagner and Nataf*, 1986]. The percent radial anisotropy is defined as

$$\xi(X, Y, Z) = 100\left(\frac{N}{L} - 1\right) \approx 200\frac{V_{SH} - V_{SV}}{V_{SV}}, \qquad (14)$$

where V_{SH} and V_{SV} are the velocities of SH and SV waves, respectively, $N = 1/8(C_{1111} + C_{2222}) - 1/4\ C_{1122} + 1/2C_{1212}$, $L = 1/2(C_{2323} + C_{1313})$, and C_{ijkl} are the coefficients of the elastic tensor of the aggregate. We calculate the elastic tensor numerically using the standard Voigt averaging formula

$$C_{ijkl} = \sum_{\nu=1}^{N} f^{\nu} a^{\nu}_{ip} a^{\nu}_{jq} a^{\nu}_{kr} a^{\nu}_{ls} c_{pqrs}, \qquad (15)$$

where N is the number of grains in the aggregate, a^{ν}_{ij} is the matrix of direction cosines for grain ν, f^{ν}

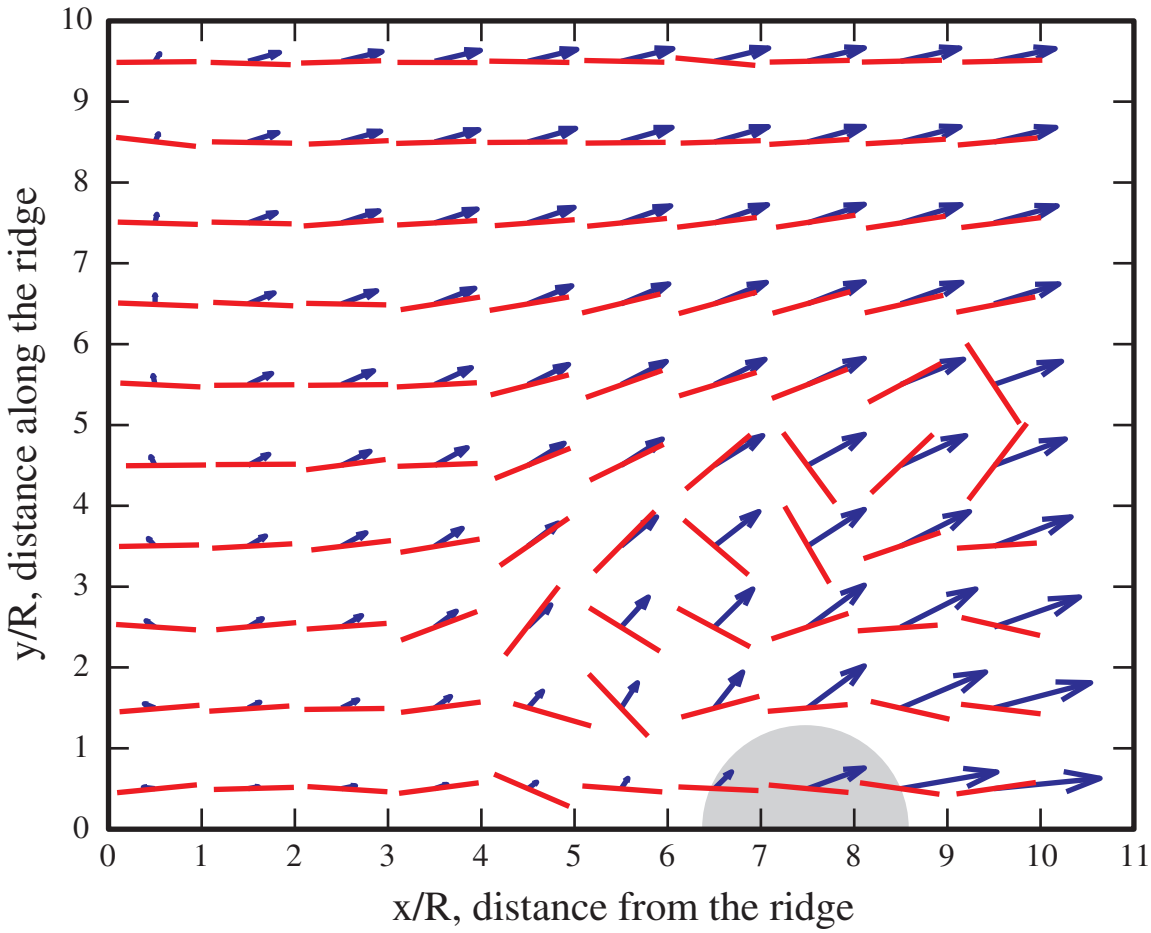

Figure 7. Horizontal velocity (arrows) and horizontal projection of the mean fast axis orientation (bars) at a depth $Z = 0.5R$ for the plume-ridge flow of Figure 5. The lattice preferred orientation is not aligned with the flow direction near either the ridge or the plume but is approximately so aligned elsewhere.

is the volume fraction of grain ν and c_{ijkl} is the single-crystal elastic tensor for olivine [*Isaak*, 1992].

[30] Figure 9 shows the radial anisotropy ξ calculated at the same depth and for the same parameters as in the previous figures.

[31] Because we consider aggregates of pure olivine, the numerically calculated values of ξ are considerably larger in absolute value than those typically observed on Earth ($\leq$ 10% [*Montagner*, 1994]). However, this does not affect the most striking feature of Figure 9, which is the change of sign of the anisotropy. Near the ridge axis, the *a* axes are subvertical, so $V_{SH} > V_{SV}$ and the radial anisotropy is negative. Near the plume and away from the ridge axis, the *a* axes are subhorizontal, implying $V_{SV} > V_{SH}$ and positive radial anisotropy. The region of large positive anisotropy delineates the parabolic shape of the flow field associated with the plume, suggesting that one may expect a clear anisotropic signature of a plume like Hawaii.

5. Discussion

5.1. LPO Development in Mantle Flow

[32] The premise of this study is that the interpretation of seismic anisotropy requires an understanding of the timescales that control its evolution in a convecting mantle. Numerical solutions of lattice preferred orientation evolution in simple uniform deformations reveal three

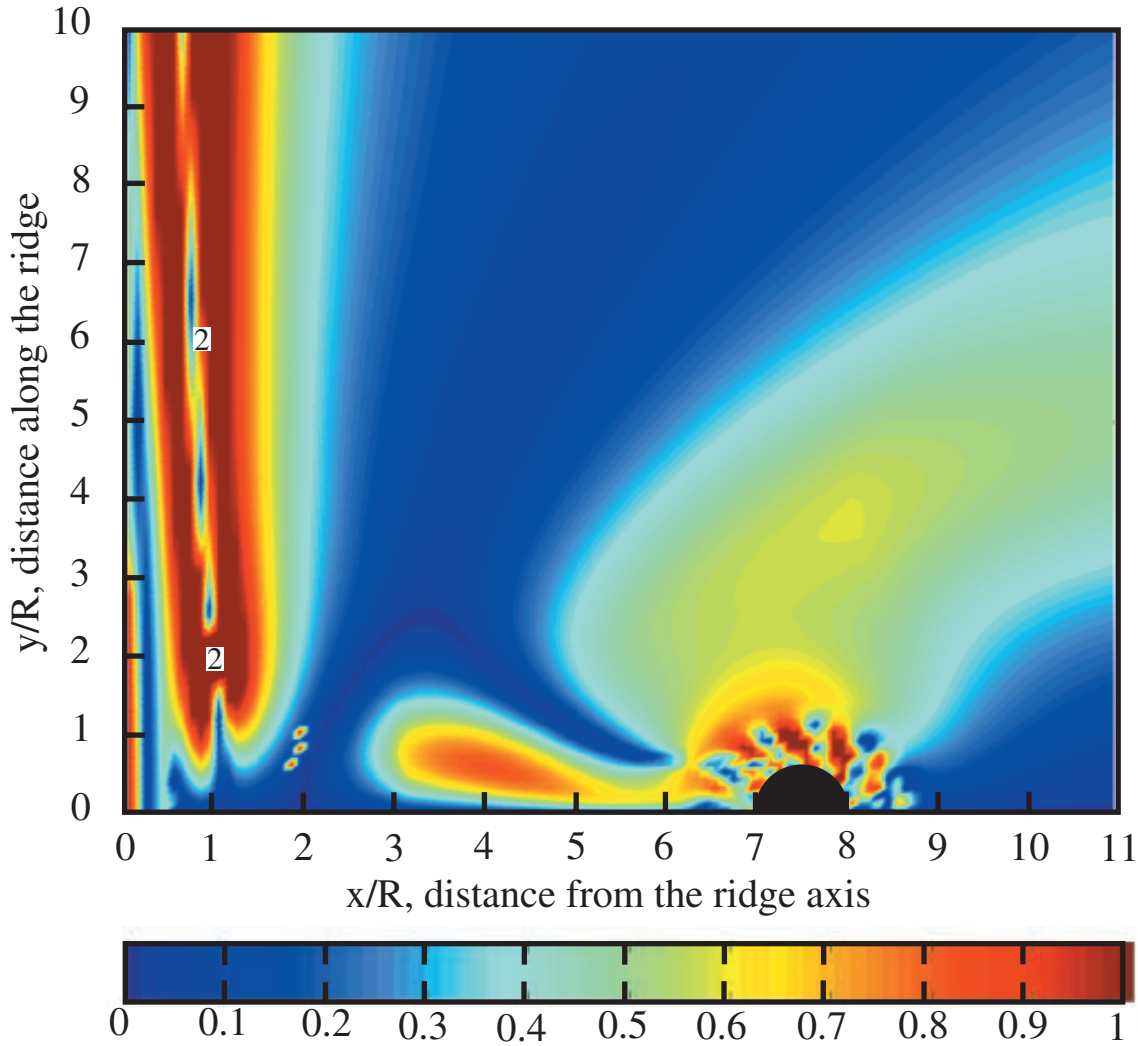

Figure 8. Orientation lag parameter $\Pi(x, y)$ at depth $z = 0.5R$ for the plume-ridge flow of Figure 6. Values $0 \leq \Pi \leq 1$ are shown by color, with locally larger values labelled. Values $\Pi \sim 2$ near the ridge axis are due to rapid change of the flow orientation from vertical to horizontal, and values $\Pi \sim 1$ in front of the plume reflect the counterflow there (Figures 6 and 7). Π is not defined in the center of the plume (black) where the vorticity is high. Large variations of Π around the plume indicate a deformation state close to uniaxial compression.

fundamental "intrinsic" timescales $\tau_{FSE} < \tau_{GBM} < \tau_{ISA}$. The most important of these is $\tau_{ISA} \sim \dot{\epsilon}^{-1}$, the time required for the mean *a* axis orientation to reach the infinite strain axis of the imposed deformation with characteristic strain rate $\dot{\epsilon}$. Two distinct results should be distinguished here: the fact that the lattice preferred orientation evolves toward the infinite strain axis and the scaling law $\tau_{ISA} \sim \dot{\epsilon}^{-1}$. Because rotation of the lattice preferred orientation toward the infinite strain axis occurs primarily by the well-understood process of intracrystalline slip, neither result depends on the model of recrystallization one uses. This is true as long as τ_{ISA} significantly exceeds the grain boundary migration timescale τ_{GBM}, which *Kaminski and Ribe* [2001]-based on available laboratory experiments-suggest to be the case.

[33] In addition to the intrinsic timescales for lattice preferred orientation evolution, nonuniformity of the flow field introduces a further "extrinsic" timescale τ_{flow} that characterizes the rate of change of the infinite strain axis itself

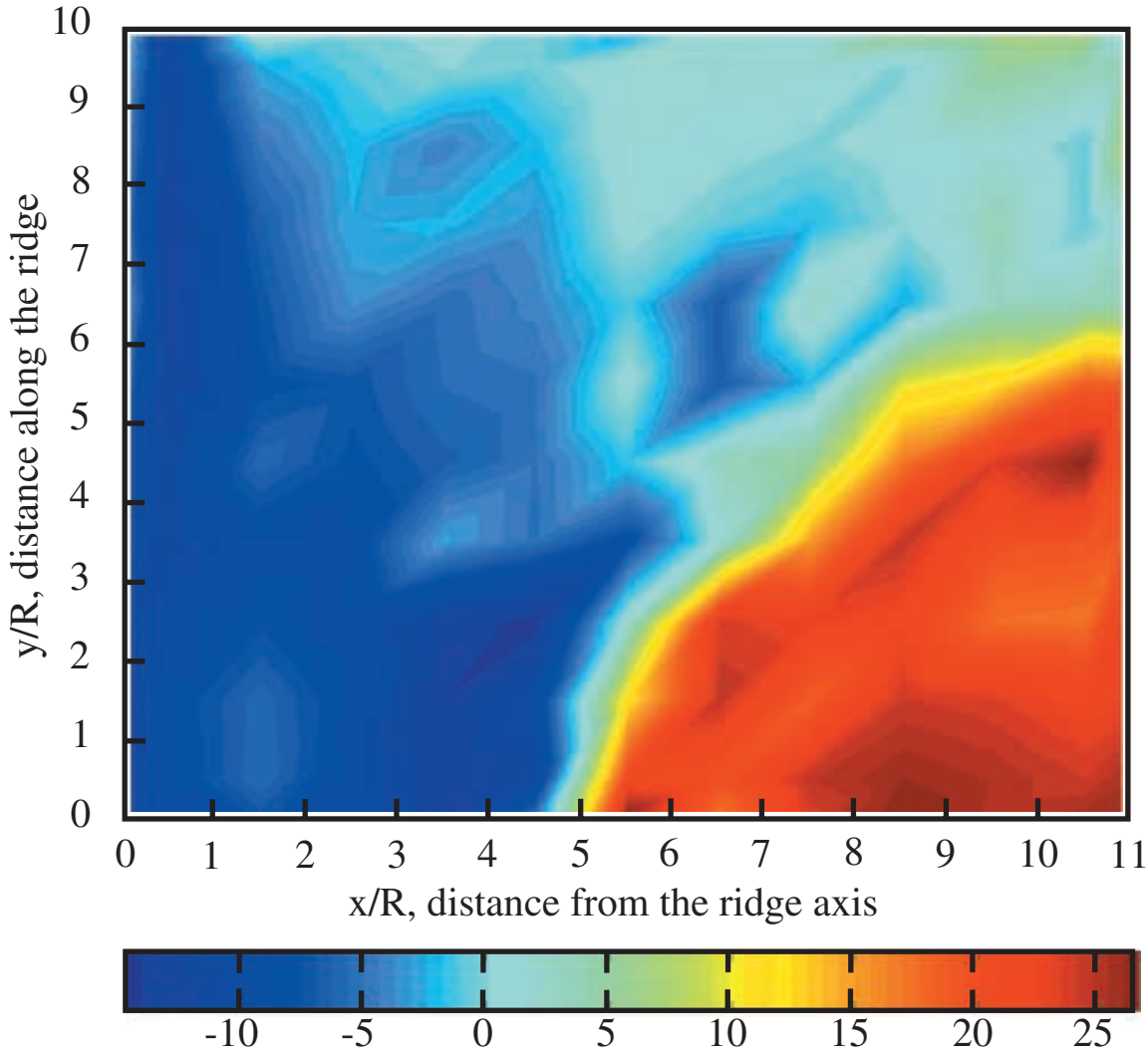

Figure 9. Radial anisotropy ξ (in percent) at depth $z = 0.5R$ for the plume-ridge model.

along path lines. One is thus naturally led to consider the ratio $\Pi = \tau_{ISA}/\tau_{flow}$ of the intrinsic and extrinsic timescales, which we have called the "grain orientation lag" parameter. At points in the flow field where $\Pi \ll 1$, the lattice preferred orientation has time to adjust to the local infinite strain axis. At points where $\Pi \gg 1$, by contrast, the lattice preferred orientation lags behind the relatively rapid changes of the infinite strain axis along path lines. Comparison of $\Pi(\mathbf{x})$ calculated from simple flow models with full numerical calculations of the lattice preferred orientation field shows that the mean a axis orientation is aligned with the flow direction only where $\Pi < 0.5$. Calculation of the lag parameter Π is thus a cost-effective way to obtain insight into the likely anisotropic structure of a candidate flow field.

[34] We picked up the infinite strain axis as one of the direction characterizing the velocity gradient tensor. One may imagine a different set of model parameters, critical shear stresses, values of M^* and of λ^*, for which the grains will align with another direction. However, this direction will still have to be a characteristic of L_{ij}, and it will thus have to follow the rotation of infinite strain axis. The value of Π obtained using infinite strain axis will be the same for any other direction characteristic of L_{ij}. For example, new simple-shear experiments indicate that olivine polycrystals deformed under water

saturated conditions may exhibit ''anomalous'' lattice preferred orientation such that the average *b* or even *c* axis is aligned with the shear direction instead of the average *a*-axis [*Jung and Karato*, 2001]. Using the model of *Kaminski and Ribe* [2001] with different activity of the slip systems to account for the effect of water we found fabrics in agreement with [*Jung and Karato*, 2001] and obtained that the lattice preferred orientation generated for various L_{ij} still rotates as the infinite strain axis [*Kaminski*, 2002]. Hence here again we can state that the value of Π and thus its significance are independent of the details of the model used.

5.2. Implications for the Interpretation of Seismic Anisotropy

[35] Our results have many implications for the interpretation of observations of seismic anisotropy. A first question concerns the significance of the direction of fast polarization revealed by surface waves or shear wave splitting measurements. Seismologists generally assume that this direction reflects either a coherent lithospheric deformation or the direction of the asthenospheric flow or a more or less complex combination of both [*Özalaybey and Savage*, 1995; *Silver*, 1996; *Savage*, 1999; *Debayle and Kennett*, 2000]. Our model suggests that matters may not be so simple. The anisotropic signature of the lithosphere is probably a frozen one and cannot be discussed in the present theoretical frame which deals mainly with timescales. In the asthenosphere, however, we have shown that the orientation of the lattice preferred orientation pattern relative to the flow direction depends on the lag parameter Π in the flow. The lattice preferred orientation tracks the flow direction only when $\Pi \ll 1$. If $\Pi > 0.5$, there is no relationship between the local flow direction and the orientation of the *a* axis of olivine. Moreover, the parameters of shear wave splitting (fast polarization direction and delay time) are usually interpreted in term of layers of constant elastic properties, which is a good hypothesis only if Π is not too large. Because the value of Π as a function of position in the mantle is not known a priori, caution should be exercised in inferring flow directions from shear wave splitting measurements. Last, seismic data are usually interpreted in term of fast polarization direction and delay time in the hypothesis of an hexagonal symmetry of the aggregate (such that the *b* axes form a girdle on the plane normal to the direction of the mean *a* axis). Such a symmetry is not naturally generated by either plastic deformation [*Tommasi et al.*, 2000] or dynamic recrystallization [*Kaminski and Ribe*, 2001]. On the contrary, the aggregates display in general a quasi-orthorhombic symmetry. Many analytical short-cuts established for an hexagonal symmetry should thus not be used.

[36] However, the two simple examples of geophysical flows we have presented in the previous section illustrate how the model of *Kaminski and Ribe* [2001] can be used to infer the link between mantle flow and seismic anisotropy. For a given 3-D mantle flow, the model can be used to calculate the lattice preferred orientation evolution of olivine aggregates along the streamlines and provides the full 3-D anisotropic structure of the domain. In particular, both the horizontal variations and the vertical variations of the anisotropy are predicted and can be compared with the information provided by both surface waves and shear wave splitting. The major interest of the model is thus to provide directly the anisotropic signature of a given flow, without the need for an a priori seismologic model such as a given number of layers with distinct average anisotropic properties. Moreover, a priori seismologic models can only be tested using measurements of anisotropy, whereas a fluid dynamics model can be tested against other sets of observations, such as gravity and topography anomalies and classical tomographic observations.

[37] *Tommasi* [1998] and later *Rümpker et al.* [1999] have illustrated how one should use models of plastic deformation to interpret large-scale upper mantle anisotropy. Both these papers and the present study suggest that the best approach to the study of seismic anisotropy may be the direct calculation of synthetic seismograms from 3-D mantle flow models. Starting with a candidate flow model, the first step would be to calculate $\Pi(\vec{x})$ at all model grid points to obtain a preliminary indication of the likely variability of seismic aniso-

tropy and its relation to the flow direction. A more refined study would then calculate the lattice preferred orientation at all grid points, determine the anisotropic elastic tensor $C_{ijkl}(\vec{x})$ using a suitable averaging scheme, and finally calculate synthetic seismograms by "shooting" elastic waves through the resulting anisotropic model domain as by *Hall et al.* [2000].

[38] Because our lattice preferred orientation evolution model is semianalytical, it can be used at very low cost to predict the seismic anisotropy associated with any mantle flow. It can be used at various scales, for example, to study the interaction of a plume and the lithosphere, to infer 3-D flows in subduction zones, or even to reinterpret global maps of azimuthal anisotropy as a function of depth in the upper mantle in terms of convective flow.

Appendix A: Calculation of ISA Orientation

[39] The orientation of the infinite strain axis, when it exists, is the steady-state orientation of the long axis of the finite strain ellipsoid in the limit of infinite strain. Following the formalism of *McKenzie and Jackson* [1983], we first calculate the deformation gradient tensor $\mathbf{F}$ by integrating the nine coupled time-evolution equations

$$\frac{\mathrm{d}\mathbf{F}}{\mathrm{d}t} = \mathbf{L}\mathbf{F} \tag{A1}$$

subject to the initial condition $\mathbf{F} = \mathbf{I}$, where $\mathbf{L}$ is the strain rate tensor and $\mathbf{I}$ is the identity tensor. The solution of this equation is [*Gantmacher*, 1989 p. 115]

$$\mathbf{F} = \exp(\mathbf{L}t) = \mathbf{I} + \mathbf{L}t + \frac{\mathbf{L}^2}{2!}t^2 + \frac{\mathbf{L}^3}{3!}t^3 + \ldots \tag{A2}$$

We then calculate the "left stretch" tensor

$$\mathbf{U} = \mathbf{F}^T\mathbf{F}, \tag{A3}$$

where $\mathbf{F}^T$ is the transpose of $\mathbf{F}$. The eigenvectors of $\mathbf{U}$ are the directions of the major axes of the finite strain ellipsoid, and the infinite strain axis is the limit as $t \rightarrow \infty$ of the eigenvector corresponding to the largest eigenvalue. As a direct numerical calculation for $t \rightarrow \infty$ is not possible, we instead perform the calculation at a dimensionless time $\tau_{\max} \equiv \dot{\epsilon} t_{\max}$ sufficiently large that the rate of change of the eigenvector does not exceed $k\dot{\epsilon}(k \ll 1)$. For plane strain deformation, the largest value of $\tau_{\max}$ is for simple shear and is $\tau_{\max} = \sqrt{1/2k - 1} = 71$ for $k = 10^{-4}$. Moreover, we found empirically that $\tau_{\max} \leq 71$ for any uniform 3-D deformation tested and for which the infinite strain axis exists. We thus chose $\tau_{\max} = 75$ for all calculations. Rotation rates in excess of $10^{-4}\dot{\epsilon}$ at $\tau_{\max} = 75$ indicates that the infinite strain axis does not exist for the velocity gradient tensor in question.

Appendix B: ISA Evolution Along Streamlines for Uniform Two-Dimensional Flows

[40] If the reference frame is the one defined by the eigenvectors of the strain rate tensor and if we choose as the origin the point where the velocity vanishes, the components of the velocity vector for a uniform two-dimensional (2-D) flow are

$$U_x = \dot{\epsilon}_o(x - \Gamma z), \quad U_z = \dot{\epsilon}_o(\Gamma x - z), \tag{B1}$$

where (x, z) are the Cartesian coordinates. The local flow direction is

$$\psi_{\mathrm{FLOW}} = \tan^{-1}\left(\frac{\Gamma x - z}{x - \Gamma z}\right) = \tan^{-1}\left(\frac{\Gamma\cos\theta - \sin\theta}{\cos\theta - \Gamma\sin\theta}\right), \tag{B2}$$

where $\theta = \tan^{-1}(z/x)$. The angle Θ between the flow direction and the infinite strain axis is

$$\Theta = \psi_{\mathrm{ISA}} - \psi_{\mathrm{FLOW}} = \frac{1}{2}\sin^{-1}\Gamma - \tan^{-1}\left(\frac{\Gamma\cos\theta - \sin\theta}{\cos\theta - \Gamma\sin\theta}\right). \tag{B3}$$

[41] The material derivative of Θ is

$$\frac{\mathrm{D}\Theta}{\mathrm{D}t} = \vec{U}.\vec{\nabla}\Theta = \frac{\sin 2\theta - \Gamma}{\Gamma^2 - 2\Gamma\sin 2\theta + 1} \tag{B4}$$

[42] If $\Pi = 0$ the material derivative of Θ is zero, which implies

$$\theta = \frac{1}{2}\sin^{-1}\Gamma. \tag{B5}$$

[43] Replacing θ by its expression in equation (B2), we obtain the local flow direction,

$$\psi_{\mathrm{FLOW}} = \tan^{-1}\left[\frac{\sin(\sin^{-1}\Gamma)}{1+\cos(\sin^{-1}\Gamma)}\right] = \frac{1}{2}\sin^{-1}\Gamma = \psi_{\mathrm{ISA}}. \tag{B6}$$

[44] For a uniform 2-D flow, the condition Π = 0 is thus both necessary (it is so always) and sufficient for the infinite strain axis to follow the flow direction.

Acknowledgments

[45] The authors thank Martha Savage, Andrea Tommasi, and an anonymous Associate Editor for their constructive reviews. Discussions with Andrea Tommasi, Shun-Ichiro Karato, and Jean-Paul Poirier have been very helpful during this study.

References

Batchelor, G. K., *An Introduction to Fluid Dynamics*, Cambridge Univ. Press, New York, 1967.

Bystricky, M., K. Kunze, L. Burlini, and J.-P. Burg, High shear strain of olivine aggregates: Rheological and seismic consequences, *Science*, *290*, 1564–1567, 2000.

Chastel, Y. B., P. R. Dawson, H. R. Wenk, and K. Bennet, Anisotropic convection with implications for the upper mantle, *J. Geophys. Res.*, *98*(B10), 17,757–17,771, 1993.

Debayle, S., and B. L. N. Kennett, The Australian continental upper mantle: Structure and deformation inferred from surface waves, *J. Geophys. Res.*, *105*(B11), 25,423–25,450, 2000.

Etchecopar, A., A plane kinematic model of progressive deformation in a polycrystalline aggregate, *Tectonophysics*, *39*, 121–139, 1977.

Gantmacher, F. R., *The Theory of Matrices*, vol. 2, Chelsea, New-York, 1989.

Hall, C. E., K. M. Fisher, E. M. Parmentier, and D. K. Blackman, The influence of plate motions on three-dimensional back arc mantle flow and shear wave splitting, *J. Geophys. Res.*, *105*(B12), 28,009–28,033, 2000.

Hess, H., Seismic anisotropy of the uppermost mantle under the oceans, *Nature*, *203*, 629–631, 1964.

Isaak, D. G., High-temperature elasticity of iron-bearing olivines, *J. Geophys. Res.*, *97*(B2), 1871–1885, 1992.

Jung, H., and S. I. Karato, Water-induced fabric transitions in olivine, *Science*, *293*, 1460–1463, 2001.

Kaminski, E., The influence of water on the development of lattice preferred orientation in olivine aggregates, *Geophys. Res. Lett.*, *29*, 10.1029/2002GL014710, in press, 2002.

Kaminski, E., and N. M. Ribe, A kinematic model for recrystallization and texture development in olivine polycrystals, *Earth Planet. Sci. Lett.*, *189*, 253–267, 2001.

Karato, S. I., Seismic anisotropy due to lattice preferred orientation of minerals: Kinematic or dynamic, in *High-Pressure Research in Mineral Physics, Geophys. Monogr. Ser.*, vol. 39, edited by M. H. Manghani and Y. Syono, pp. 455–471, AGU, Washington, D. C., 1987.

Karato, S. I., and K. H. Lee, Stress-strain distribution in deformed olivine aggregates: Inference from microstructural observations and implications for texture development, *Proceedings of the ICOTOM*, *12*, 1546–1555, 1999.

McKenzie, D. P., Finite deformation during fluid flow, *Geophys. J. R. Astron. Soc.*, *58*, 689–715, 1979.

McKenzie, D. P., and J. Jackson, The relation between strain rates, crustal thickening, paleomagnetism, finite strain and fault movements within a deforming zone, *Earth Planet. Sci. Lett.*, *65*, 182–202, 1983.

Montagner, J. P., Can seismology tell us anything about convection in the mantle?, *Rev. Geophys.*, *32*(2), 115–138, 1994.

Montagner, J. P., Where can seismic anisotropy be detected in the earth's mantle? In boundary layers, *Pure Appl. Geophys.*, *151*, 223–256, 1998.

Montagner, J. P., and H. C. Nataf, On the inversion of the azimuthal anisotropy of surface waves, *J. Geophys. Res.*, *91*, 511–520, 1986.

Nicolas, A., and N. I. Christensen, *Formation of anisotropy in upper mantle peridotites: A review*, in *Composition, Structure and Dynamics of the Lithosphere-Asthenosphere System, Geodyn. Ser.*, vol. 16, edited by K. Fuchs and C. Froidevaux, pp. 111–123, AGU, Washington, D. C., 1987.

Nicolas, A., F. Boudier, and A. M. Boullier, Mechanisms of flow in naturally and experimentally deformed peridotites, *Am. J. Sci.*, *273*, 853–876, 1973.

Özalaybey, S., and M. K. Savage, Shear-wave splitting beneath western United States in relation to plate tectonics, *J. Geophys. Res.*, *100*(B9), 18,135–18,149, 1995.

Podzrikidis, C., *Introduction to Theoretical and Computational Fluid Dynamics*, Oxford Univ., New York, 1997.

Poirier, J.-P., *Creep of Crystals*, Cambridge Univ., New York, 1985.

Ribe, N. M., On the relation between seismic anisotropy and finite strain, *J. Geophys. Res.*, *97*(B6), 8737–8747, 1992.

Ribe, N. M., and U. R. Christensen, The dynamical origin of hawaiian volcanism, *Earth Planet. Sci. Lett.*, *171*, 517–531, 1999.

Ribe, N. M., and Y. Yu, A theory for plastic deformation and textural evolution of olivine polycrystals, *J. Geophys. Res.*, *96*, 8325–8335, 1991.

Rümpker, G., A. Tommasi, and J.-M. Kendall, Numerical simulations of depth-dependent anisotropy and frequency-dependent wave propagation, *J. Geophys. Res.*, *104*(B10), 23,141–23,153, 1999.

Russo, R. M., and P. G. Sylver, Trench-parallel flow beneath the Nazca plate from seismic anisotropy, *Science*, *263*, 1105–1111, 1994.

Savage, M. K., Seismic anisotropy and mantle deformation: What have we learned from shear wave splitting, *Rev. Geophys.*, *37*(1), 69–106, 1999.

Silver, P. G., Seismic anisotropy beneath the continents: Prob-

ing the depths of geology, *Annu. Rev. Earth Planet. Sci.*, *24*, 385–432, 1996.

Tommasi, A., Forward modeling of the development of seismic anisotropy in the upper mantle, *Earth Planet. Sci. Lett.*, *160*, 1–18, 1998.

Tommasi, A., D. Mainprice, G. Canova, and Y. Chastel, Viscoplastic self-consistent and equilibrium-based modelling of olivine lattice preferred orientations, 1, Implications for the upper mantle seismic anisotropy, *J. Geophys. Res.*, *105*(B4), 7893–7908, 2000.

Wenk, H. R., and C. N. Tomé, Modeling dynamic recrystallization of olivine aggregates deformed in simple shear, *J. Geophys. Res.*, *104*(B11), 25,513–25,527, 1999.

Wenk, H. R., K. Bennett, G. Canova, and A. Molinari, Modelling plastic deformation of peridotite with the self-consistent theory, *J. Geophys. Res.*, *96*, 8337–8349, 1991.

Zhang, S., and S. I. Karato, Lattice preferred orientation of olivine aggregates deformed in simple shear, *Nature*, *375*, 774–777, 1995.

Zhang, S., S. I. Karato, J. F. Gerald, U. H. Faul, and Y. Zhou, Simple shear deformation of olivine aggregates, *Tectonophysics*, *316*, 133–152, 2000.